The SPARC_LAB Thomson Source

C. Vaccarezza[a,1], D. Alesini[a], M.P. Anania[a], A. Bacci[d], A. Biagioni[a], F. Bisesto[a], M. Bellaveglia[a], P. Cardarelli[c], F. Cardelli[f], A. Cianchi[g], E. Chiadroni[a], M. Croia[a], A. Curcio[a], P. Delogu[e], D. Di Giovenale[a], G. Di Domenico[c], G. Di Pirro[a], I. Drebot[d], M. Ferrario[a], F. Filippi[f], A. Gallo[a], M. Galletti[a], M. Gambaccini[c], A. Giribono[f], B. Golosio[b,h], W. Li[a], A. Mostacci[f], P. Oliva[b,h], D. Palmer[d], V. Petrillo[d], M. Petrarca[c], S. Pioli[a], L. Piersanti[f], R. Pompili[a], P. Oliva[b,h], S. Romeo[a], A.R. Rossi[d], J. Scifo[a], L. Serafini[d], G. Suliman[i], F. Villa[a]

[a] *INFN-LNF, Via Enrico Fermi,40 00044 Frascati Rome, Italy*
[b] *INFN-CA, Complesso Universitario di Monserrato, S.P. per Sestu km 0.700,Cagliari, Italy*
[c] *University of Ferrara and INFN-FE, via Saragat 1, 44122 Ferrara, Italy*
[d] *INFN-MI, Via Celoria 16, 20133 Milan, Italy*
[e] *University of Pisa and INFN-PI,Largo B. Pontecorvo 3, 56127 Pisa, Italy*
[f] *University La Sapienza and INFN-Roma1, Piazzale Aldo Moro,2 00161 Rome, Italy*
[g] *University of Rome Tor Vergata, Via della Ricerca Scientifica 1, 00133 Rome, Italy*
[h] *University of Sassari,Piazza Universit 21, 07100 Sassari, Italy*
[i] *IFIN-HH,Str. Reactorului no.30, P.O.BOX MG-6, Bucharest - Magurele, Romania*

Abstract

The SPARC_LAB Thomson source is a compact X-rays source based on the Thomson backscattering process presently under its second phase of commissioning at LNF. The electron beam energy ranges between $30-150MeV$, the electrons collide head-on with the Ti:Sapphire FLAME laser pulse which energy ranges between $1-5J$ with pulse lengths in the $0.1-10psec$ range, this provides an X-rays energy tunability in the range of $20-500keV$, with the further capability to generate strongly non-linear phenomena and to drive diffusion processes due to multiple and plural scattering effects. The experimental results on the obtained X-ray radiation are presented.

Keywords: `elsarticle.cls`, LaTeX, Elsevier, template
2010 MSC: 00-01, 99-00

1. Introduction

The second commissioning shift of the SPARC_LAB Thomson source took place in June 2015 aiming to improve the photon flux measured in the very first attempt of Compton collisions in 2014. The SPARC_LAB Thomson source has been described elsewhere [1] and it consists in the SPARC photoinjector [2, 3], that provides the $30 \div 150MeV$ electron beam, coupled with the $300TW$ FLAME laser system [3, 4] in order to provide a X-ray Thomson source in the range of $20 \div 500keV$. A $20m$ double

[1] Email address: cristina.vaccarezza@lnf.infn.it

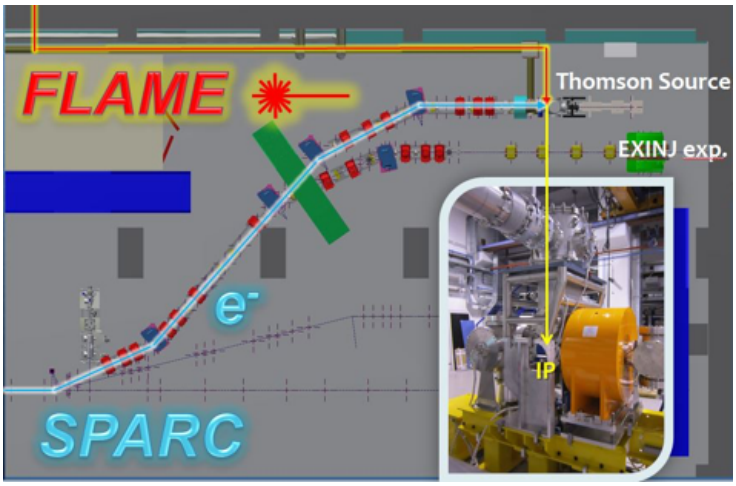

Figure 1: SPARC_LAB Thomson source schematic layout.

dogleg carries the electron beam output from the photo injector down to the Thomson Interaction Point where the FLAME laser pulse is brought by a $20m$ in vacuum optical transfer line, see Fig. 1. Since the first planned experiment with the Thomson radiation was the X-ray imaging of mammography phantoms with phase contrast technique[5, 6, 7], the source parameters of the electron and laser beams have been so far optimized to obtain the required flux of photons with moderate (20%) monochromaticity and are reported in Table1. For this commissioning phase anyway more relaxed parameters have been adopted and the obtained results are described in the following sections of this paper. Nevertheless is worth to notice the relevance of the SPARC_LAB Thomson source in terms of energy tunability that, for example, will provide the possibility to explore the ELI-NP Gamma Beam Source low energy range operation, since the electron beam energy is foreseen to range between 75 and 740 MeV. Certainly the opportunity to test the electron beam dynamics together with the electron and radiation diagnostic will play an important role in view of the ELI-NP machine future commissioning in Magurele under the INFN responsability. Moreover thanks to the FLAME laser system flexibility non linear regimes for the Compton scattering could be explored together with new experimental schemes that conjugate the Compton radiation production with the most advanced plasma based acceleration schemes for the electrons.

2. The Electron Beam

The electron beam is provided by a 1.6 cell S-band RF gun equipped with a Cu photocathode driven by a $50\mu J$ Ti:Sapphire laser and a four coils solenoid for the emittance compensation. The beam is then accelerated by three TW SLAC type S-band linac sections (S1-S3) up to the desired energy. At the exit of the linac a 6D beam

Table 1: Thomson Source Design Parameterst

Electron Beam	Energy	(MeV)	30
	Energy spread	%	< 0.1
	Charge	(pC)	$100 \div 800$
	Emittance	(mm mrad)	$1 \div 3$
Laser Beam	Wavelenghth	(nm)	800
	Pulse energy	(J)	$1 \div 5$
	Pulse length	(ps)	10
	Spot size	(μm)	10
	Repetition rate	(Hz)	10
X-ray Beam	Photon energy	(keV)	$20 \div 500$
	Photon number per shot		10^9
	Source rms radius	(ps)	10
	Bandwidth	%	$10 \div 20$

phase space measurement system is available [8] by means of a S-band RF deflecting cavity and a 14 deg bypass dipole employed also for energy and energy spread measurements. The working point for this second commissioning phase has been set up with $Q = 200pC$ beam and energy $E = 30MeV$. No RF attenuators are available in the RF systems of the three S-band TW sections that follow the gun, therefore an hybrid compression-deceleration scheme has been set with the following phases of the accelerating sections: $\Phi S1 = +32deg$, $\Phi S2 = -72deg$, $\Phi S3 = -134deg$ from crest, in order to minimize the effects of the power amplitude jitter from the feeding Klystrons, and obtain a final energy of $30MeV$ with an energy spread $\sigma_\delta \leqslant 0.1\%$. The envelope and beam emittance evolution through the photoinjector has been simulated with the ASTRA [9] and 50k particles; the results are shown in Fig. 2 and are in good agreement with the beam spot measurements (reported dots, crosses) taken at the screen locations along the linac. The longitudinal space of the electron beam at the exit of the photoinjector is measured by means of the S-band RF deflector coupled with a 14 dipole magnet and is reported in Fig. 3 as captured on the YAG screen located downstream the dipole.

From the photoinjector exit a double dogleg with a final two branch interaction zone brings the electron beam to the interaction points of the Thomson and the plasma acceleration external injection experiment, see Fig. 1. The R_{56} parameter can be set in the range of 50 mm, closing the horizontal dispersion at the end of the last dogleg dipole. For the commissioning phase the dispersion is closed at the end of each dipole pair and the emittance evolution measurement is performed with the quadrupole scan technique in each straight section downstream the dipole pairs [1]. From the transverse emittance measurement performed at the linac exit the Twiss parameters are obtained to match the beam to the dogleg entrance for the transport to the Interaction Point. The final focusing is performed in the final straight section using a quadrupole magnet triplet and a solenoid, with a maximum field B=1.1T, close to the IP. At 30 MeV the minimum obtained spot size for the electron beam was around $\sigma_{rms} \approx 60 \div 80\mu m$ as

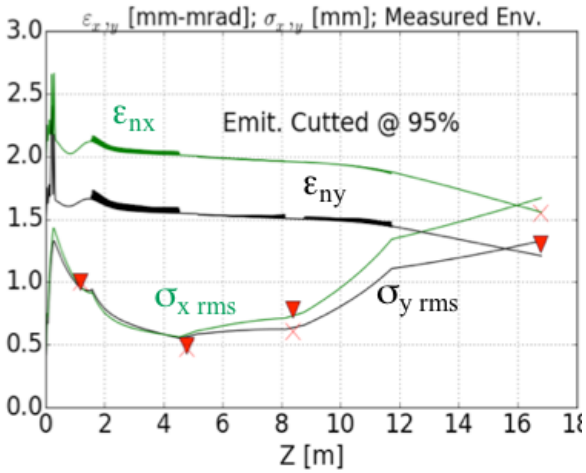

Figure 2: Electron beam emittance (hor, vert) and envelope (x,y) evolution from the photocathode to the linac exit calculated with the Astra code (Full 3D analysis). The dots and crosses represent the beam spot measurements (horizontal and vertical) taken in these configurations at screen locations along the linac.

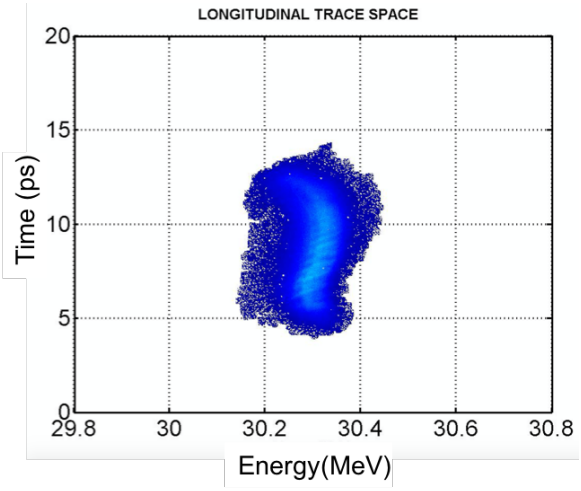

Figure 3: Longitudinal phase space image of the 30*MeV* electron beam coming out the SPARC photoinjector.

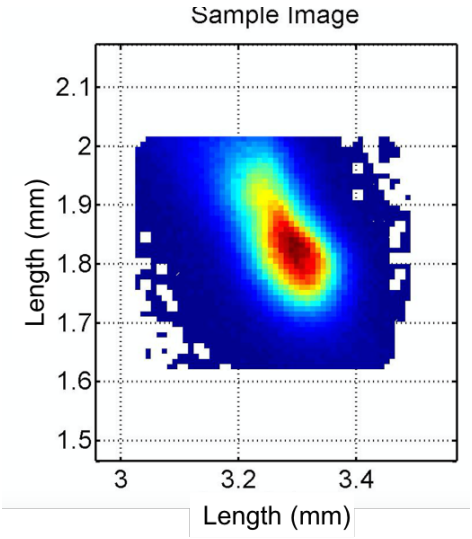

Figure 4: Electron beam spotsize at the IP, with $\sigma_{rms} \approx 60 \div 80 \mu m$, vertical and horizontal respectively.

reported in Fig. 4.

3. The Photon Beam

The laser pulse used to drive the Thomson back scattering process with the SPARC electron beam is provided by the FLAME laser system [4]. FLAME is a nominal $300TW$ laser system that uses 11 YAG pump lasers and 5 titanium-sapphire multi-pass amplifiers to produce linearly polarized pulses with a central wavelength $\lambda_0 = 0.800 \mu m$ in a $60 \div 80nm$ bandwidth. The pulse duration ranges between $25fs \leqslant \tau_L \leqslant 10ps$, and the maximum energy is $E = 7J$ that corresponds to an energy on target $E_t \sim 5J$, at $10Hz$ repetition rate. The laser system is hosted in a clean room at the ground floor of the FLAME building and is optically transported in a shielded underground area where the compressor is located and that is adjacent to the SPARC hall. From here an optical transfer line in vacuum, ($P = 10^{-6} Torr$), carries the beam up to the parabolic mirror of the Thomson interaction chamber, see Fig.5, that focuses the beam in a $10 \mu m$ diameter (FWHM) spot at the interaction point. The required focal spot has been obtained with the use of the adaptive optic placed inside the compressor. This mirror is used to control the phase-front of the photon beam. Figure 6 shows two images of phase front measurement: the one on the left hand side, is the phase front measured without any correction which shows a large aberration (the rms error respect to a perfect spherical phase front of about 2 micron) and the one on the right hand side shows a corrected phase front which shows almost no aberrations (the error this time is only $50nm$).

The corresponding beam at the focus (Thomson IP) for these two different phase fronts are imaged in Fig.7. The beam is quite oval in the case of no phase front correction and becomes nearly round when the best phase front is applied. Moreover, it is

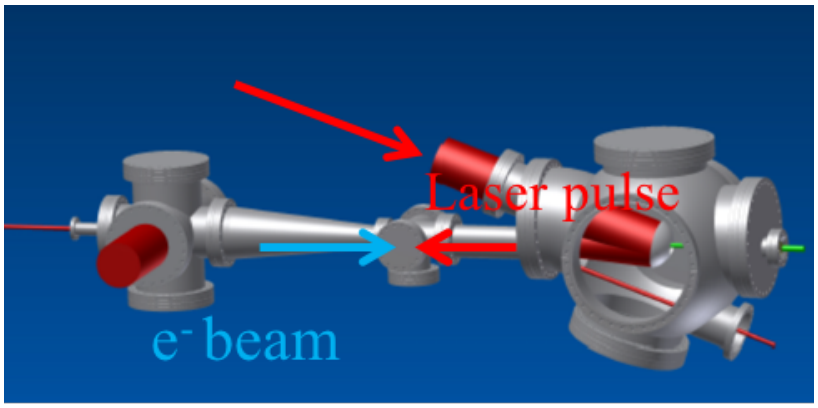

Figure 5: 3D CAD drawing of the Thomson Interaction vacuum chamber setup.

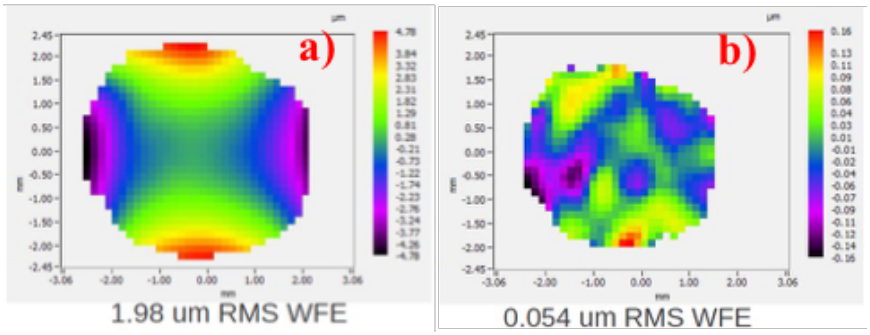

Figure 6: Phase front error measured (a) before phase front correction and (b) after correction showing an rms error respect to a perfect spherical phase front of (a) $1.98\mu m$ and (b) $0.054\mu m$.

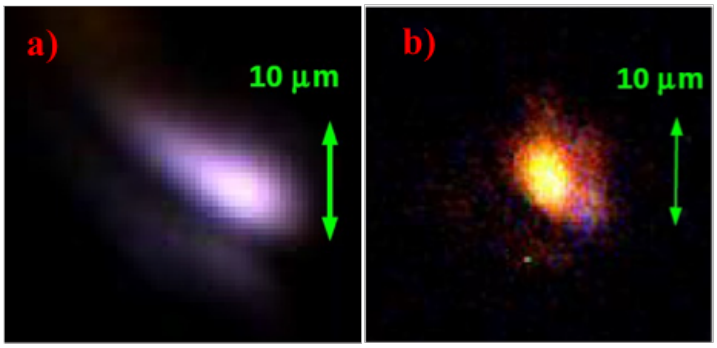

Figure 7: FLAME focal spot (a) without phase front correction and (b) with phase front correction.

perceptible that the use of the adaptive optics is crucial also for the energy contained in the central spot (considering the $1/e^2$ diameter): in fact, when there is no phase front correction, the energy inside the central spot is only 25% while after the phase front correction, this energy is 60%.

4. Synchronization

The Thomson scattering experiment needs an extremely precise synchronization between electron bunch and laser pulse. The electrons and the photons collide well inside the waist region of the laser beam final focus provided that the relative time of arrival jitter at the IP between the two beams is $\leqslant 500 fs_{RMS}$. The electrons are generated by photo-emission from a copper cathode hit by an UV pulse produced by a dedicated laser system (the photo-cathode laser), then they are captured and accelerated by the RF fields of the RF gun and traveling wave accelerating sections. Then the bunch time of arrival at the IP depends on the arrival time of the laser on the photocathode and on the phase of the RF accelerating fields. The arrival time at the IP of the extremely intense IR laser pulse depends on the starting time of the seed pulse, which is selected from a laser oscillator pulse train and then amplified, compressed and transported. The synchronous arrival of electrons and photons at the IP is obtained by locking the oscillators of the photo-cathode laser and interaction laser systems, and the phase of the RF accelerating fields to a common Reference Master Oscillator (RMO). The RMO is a low phase noise ($60 fs_{RMS}$ integrated in the $10Hz \div 10MHz$ range) microwave oscillator tuned at the Linac main frequency 2856 MHz. The laser oscillators are locked through a PLL architecture to the 36th sub-harmonics of the RMO, while the output RF phase of the linac klystrons is downconverted to baseband by mixing with the RMO signal, and deviations are corrected both within the $4\mu s$ RF pulse duration (jitter feedback) and pulse-to-pulse (drift feedback).

The measured synchronization performances of the main SPARC_Lab subsystems are reported in 4. The jitter of the bunch arrival time at the end of the linac has been measured relative to the klystron RF streaking the bunch on a screen by means of

Table 2: Measured synchronization performances of the main SPARC_Lab sub-systems

System	Measured jitter	Note
Reference Master Oscillator	$\approx 60 fs_{RMS}$	Absolute, $10Hz \div 100MHz$
Photo-Cathode Oscillator	$\approx 50 fs_{RMS}$	Absolute, $10Hz \div 100MHz$
Interaction Laser Oscillator	$\approx 100 fs_{RMS}$	Absolute, $10Hz \div 100MHz$
RF Output Klystron 1,2	$\approx 50 fs_{RMS}$	Relative to RMO, average over the pulse
Electron Bunch	$< 100 fs_{RMS}$	Relative to RF (meas. with RF deflector), Relative to photocathode laser (meas. with EOS)

an RF deflecting cavity and recording shot to shot the bunch centroid vertical position. In alternative the bunch arrival time has been measured relative to the photocathode laser using the Electro Optical Sampling technique [10]. The measured jitter of the bunch arrival time is $< 100 fs_{RMS}$ with both methods, that in our implementation present a similar estimated resolution of $\approx 20 fs_{RMS}$. Once locked to the RMO, the measured absolute integrated phase noise of the interaction laser FLAME oscillator is $\approx 100 fs_{RMS}$, and we do not expect significant performance degradation by the laser amplification and transport. So the expected relative jitter of the arrival time at IP of electron bunch and laser pulse is well below the $500 fs_{RMS}$ specification. In 8 (above) the control window of the PLLs implemented on the photo-cathode and interaction lasers is shown. Once locked both to the RMO, the window gives the possibility of freely phasing the two systems at any desired position. Figure 8 (below) shows the signals induced by electron and photon pulses in pick-ups placed close to the IP. Taking into account the time-of-flight from pick-up to IP, this measurement allows a coarse temporal pre-alignment of the beams, while a fine temporal superposition can be found experimentally by maximizing the flux of the Thomson radiation.

5. X-ray beam Diagnostic

To verify the collision alignment and synchronisation the x-ray detection is a fundamental diagnostic tool. In the commissioning phase a detector that allows to measure the x-ray yield is required that must have a high sensitivity and a wide dynamic range to detect the potentially weak signal generated in the first non-optimised collisions. The detector we selected is a scintillator crystal coupled with a photomultiplier tube (PMT) located at $450cm$ downstream the Thomson IP. The crystal used is a CsI(Tl) of size (20x20x2) mm^3, coupled with a light-guide to a PMT (Hamamatsu, mod. R329-02). The signal is acquired using both an oscilloscope and a multichannel analyser (MCA-8000, Amptek, US) connected to a PC. Due to the high intensity and short duration of the pulse, it is not possible to distinguish the signal produced by the interaction of each single photon in a pulse, as in traditional spectroscopic application, but the signal is proportional to the entire energy released in the scintillator by each pulse. Therefore, an information on the energy distribution is required to evaluate the number of photon

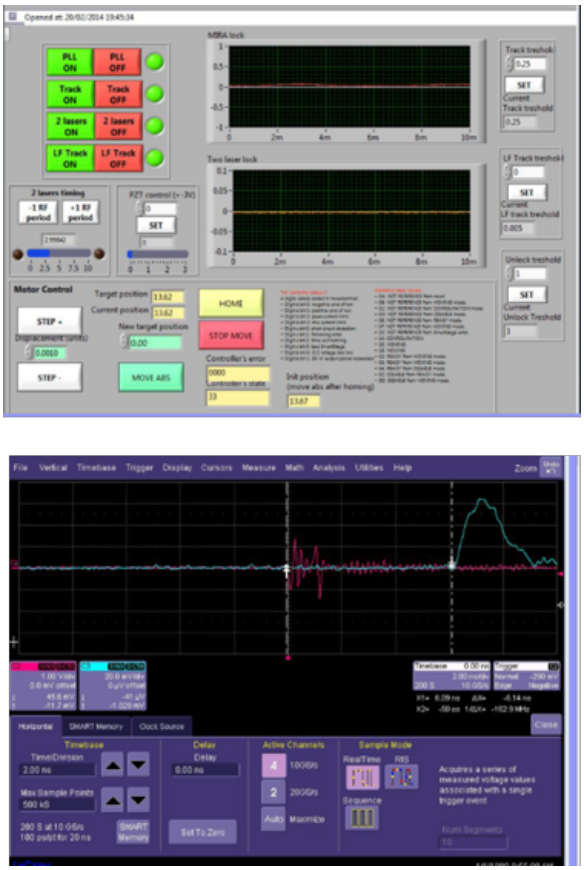

Figure 8: above: Control window of PLL of the 2 lasers; below: Screenshot of signals induced by the electron and photon pulses passing near the IP.

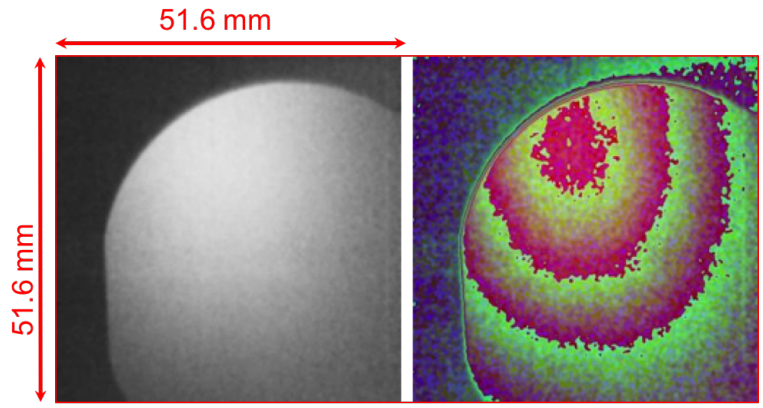

Figure 9: Thomson X-radiation image collected with Hamamatsu imager Flat Panel C9728DK-10, located at 300cm from the IP, with 1s exposure time and averaged over 100 images.

in each pulse. To calibrate the detector response, the signal produced by two radioactive sources: Am-241 (59.54 keV) and Cs-137 (662 keV) was performed as a function of the HV applied and the amplificator gain; adjusting the HV and gain it is possible to detect signals in a wide range. In addition to the PMT described, the beamline is equipped with a set of Si PIN diode detectors, previously calibrated with monochromatic synchrotron light, located at 200 and 300 cm from IP respectively, that together with an X-ray imager and techniques specifically developed [11, 7], allow a full characterization of the x-ray source in terms of flux, energy distribution, spatial distribution and beam stability.

6. Commissioning results

For this second commissioning phase a 200pC electron beam at 30 MeV has been selected as working point. At the Linac exit the measured normalized transverse emittance was $\varepsilon_{x-y} = 1.2 - 2.2 \pm 0.2 \mu rad$, with an energy spread $\sigma_\delta = 0.1 \pm 0.03\%$, and a rms length $\sigma_z = 2.2 \div 0.2 ps$. The minimum electron beam size reached was $\sigma_{x-y} \sim 60 - 80 \pm 10 \mu m$. Due to background problems on the X-ray detectors, placed relatively close to the electron beam dumper, we should limit the IP electron spot size to $\sigma_{x-y} \sim 110 \pm 10 \mu m$. In fact, due to a residual misalignment of the electron beam with the respect to the dumper vacuum pipe (enhanced by the strong focusing field of the solenoid B = 0.7 T), the background increased when the beam divergence was higher as consequence of a stronger focusing at IP. This misalignment was also detected by the imager recorded data that are shown in Fig.9 where the Thomson radiation image is clearly cut by the Perspex CF 40 window profile.

To measure the radiation energy two k-edge filters, Nb and Zr, were also used, resulting in a roughly estimated value of 13 keV, confirming the cut of the most energetic part of the produced radiation due to the tilted electron trajectory. In fact, with our

commissioning setup the expected number of photons in the 20% bandwidth is:

$$N_\gamma = 4.8 \times 10^8 \frac{U_L[J]Q[pC]\delta_\phi}{h\nu[eV](\sigma_x^2[\mu m] + \frac{w_0^2[\mu m]}{4})} \approx 1.4 \times 10^6 photons/shot \quad (1)$$

with $U_L \approx 2J$, $Q \approx 200pC$, $\delta_\varphi = 0.2$, $h\nu = 1.55eV$, $\sigma_{x,y} \approx 110\mu m$ and $w_o \approx 150\mu m$ while our measured photon flux is $N_\gamma \approx 10^4 photons/pulse$.

Another contribution to the reduction of the obtained photon flux can also come from the jitter sensitivity of our $30MeV$ working point, deeply off crest in the S-band accelerating sections, as coming out from the simulation results shown in Fig.10, where the Thomson radiation spectrum is shown as calculated with CAIN code starting from the measured parameters for the electron and photon beams (Fig.10 above) and its sensitivity to the jitter of electron beam horizontal centroid is shown in terms of photon flux reduction (Fig.10 below).

7. Conclusions

The second commissioning phase of the SPARC_LAB Thomson source took place in the June 2015 dedicated shift. The 30 MeV electron beam energy WP has been addressed as foreseen for the first planned imaging experiment. With the available hardware (only phase shifters on the 3 TW S-band sections) the applied acceleration/deceleration scheme worked well enough to produce a low energy spread electron beam at 30 MeV, even though resulting in a strong sensitivity for the electron beam to the machine imperfections/stability. The optimization plan foresees a better control of the electron trajectory at the IP to avoid unrecoverable off-axis emission of the Thomson radiation and too high background contribution to the X-ray detectors signal. An interaction setup upgrade is also under study, coming to an non-zero angle collision in order to make it easier the electron and laser pulse trajectory control removing the on axis counter propagation that limit the room availability for both beams diagnostic.

8. References

[1] C. Vaccarezza, et al., IPAC 14 Dresden, Germany (2014) 267–269.

[2] M. Ferrario, et al., Nuclear Instr. and Meth. in Phys. Res. B 309 (2013) 183–188.

[3] M. Ferrario, et al., IPAC 10 Kyoto, Japan.

[4] L. Labate, et al., Radiation Effects and Defects in Solids 165.

[5] A. Bacci, et al., Nuclear Instr. and Meth. in Phys. Res. B 608 (2009) 90–93.

[6] P. Oliva, et al., Nuclear Instr. and Meth. in Phys. Res. A 615 (2010) 93–99.

[7] B. Golosio, et al., Applied Physics Letters 100 (164104).

[8] D. Alesini, et al., Nuclear Instr. and Meth. in Phys. Res. A 568 (2006) 488–502.

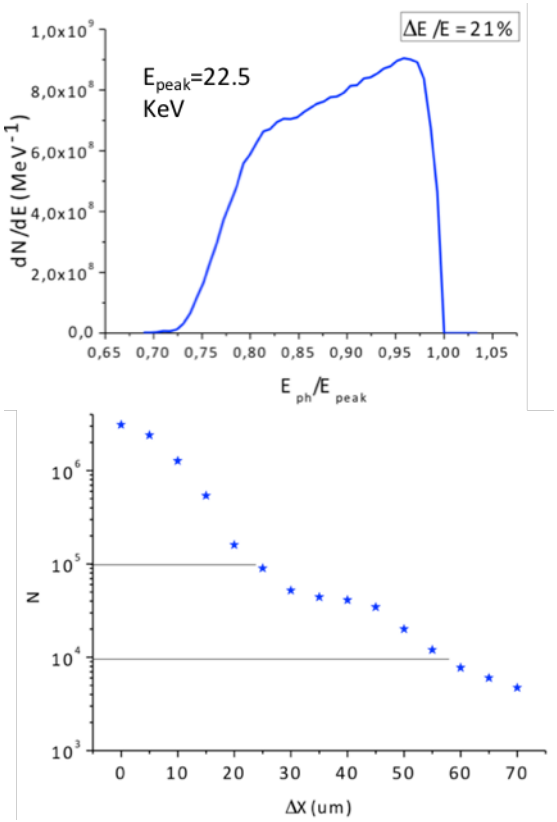

Figure 10: Thomson X-radiation spectral distribution calculated from the measured electron and laser beam parameters for this second commissioning shift (above), the relative photon flux reduction estimation coming from the jitter in the transverse electron beam centroid.

[9] K. Flottmann, http://www.desy.de/ mpyflo/.

[10] R. Pompili, et al., Nuclear. Instr. and Meth. in Phys. Res. A 740 (2014) 216–221.

[11] P. Cardarelli, et al., Journal of Applied Physics 112 (074908).